




On-machine tool wear estimation using a portable digital holographic camera

Gaurav Dwivedi^{1,2} · Lavlesh Pensia^{1,2} · Omendra Singh¹ · Raj Kumar^{1,2} 

Received: 22 December 2021 / Accepted: 1 March 2022 / Published online: 24 March 2022
© The Author(s), under exclusive licence to Springer-Verlag GmbH Germany, part of Springer Nature 2022

Abstract

Machine tools are integral part of the machining process and they require regular monitoring for detection of wear of the tool to control the surface finish of the machined products, e.g., mechanical and optical components and assemblies. In this work, we report application of an indigenously developed compact and portable digital holographic camera for wear inspection and metrology of cylindrical end mill and square shoulder face mill machine tools. The camera utilises principles of digital holographic interferometry for wear inspection. It provides direct access to the complex amplitude of light scattered from the test object, which makes the camera suitable for quantitative analysis of irregularities present on the test surface. Wear as well as cracks in the tools incurred during machining process are analysed qualitatively as well as quantitatively by applying the digital holographic interferometry technique. The developed digital holographic camera is also suitable for in-situ inspection of machine tools. The experimental results are validated by a standard mechanical profiler and a measurement error of around 9% is reported. The results presented in this manuscript can be of significant importance in deciding the tool replacement time in the machining process based on the acceptable quantitative value of wear.

1 Introduction

Precision and accuracy of machined workpieces are highly desirable in several manufacturing industries such as automotive, aerospace, medical, optical, electronics, communications, defense etc. [1]. Quality of machined components depends on several parameters of the machining process such as numerical control of machine tools, proper execution of manufacturing steps, durability of machine tools, geometric errors, and thermal effects of the machine etc. [2]. Direct interaction of machine tools such as drill, lathe, mill etc. with the workpiece makes them one of the important components to be regularly inspected for the occurrence of any wear or deformity during machining processes [3, 4]. Wear in machine tools can be defined as the gradual deterioration of their cutting edges due to constant and rigorous operation. These wear are commonly caused by extreme physical stress and temperature generated during the machining process [5]. Different types

of tool wear are classified according to affected region of the tool, e.g. [6], flank wear, crater wear, notch wear, nose radius wear, thermal and mechanical cracking, edge buildup, plastic deformation, and edge chipping etc. Usually, machine tools are replaced after a fixed time duration provided by the manufacturer, even though certain useful lifetime may be left in them. Thus, to optimize productivity of the machine tools and to observe tool wear, non-contact inspection techniques are required. The on-machine inspection methods of tool wear can be categorized into direct methods and indirect methods [7]. The indirect methods predict tool wear by utilizing parameters such as motor current, cutting force, vibration, torque, acoustic emission etc. [8]. These methods lack in providing information of actual tool wear and are sensitive to environmental changes [9]. On the other hand, the direct methods are more reliable and flexible as they can directly measure the actual tool wear. An example of direct method is visual inspection. Due to subjective nature, visual inspection of machine tools is prone to certain human errors [10]. Methods based on machine vision [11, 12], laser projection [13, 14], laser scanning confocal microscope [15], white light interferometry [16], stereo vision system [17], finite element method [18], conoscopic holography [19], acoustic emission [20, 21], accelerometer [22] etc. are also reported in the literature. Digital holographic interferometry (DHI) [23] is another direct method which has

✉ Raj Kumar
raj.optics@csio.res.in

¹ CSIR-Central Scientific Instruments Organisation,
Chandigarh 160030, India

² Academy of Scientific and Innovative Research (AcSIR),
Ghaziabad 201002, India

the capability to simultaneously access latitudinal and longitudinal dimensions of a test object. DHI technique is used in several applications, including detection and measurement of surface non-uniformities like scratch, cracks, delamination etc. [24–27], study of thermal and mechanical stresses and strain distribution [28, 29], shape and thickness measurements [30, 31], inspection of printed circuit boards [32, 33], vibration analysis [34], observation of deformation of tooth model in real time [35], tableware and wood inspection [36, 37] etc. Although DHI suffers from small field of view, and high vibration sensitivity; the setup can be improved to overcome these shortcomings. In an effort to achieve it, we developed a compact and portable setup based on optical digital holography with extended field of view and high temporal stability [38, 39]. The developed setup has been successfully utilized for several non-contact inspection applications [36, 38].

Present work reports on-machine inspection of machine tools used on the milling machine, to detect the presence of wear incurred during the machining process, using a portable digital holographic camera [38]. Inspection is performed by applying optical digital holography [40] based non-destructive testing technique, which utilizes the principle of digital holographic interferometry (DHI) [41]. DHI is benefitted by the merits of digital holography, which could provide direct access to amplitude and phase of light modulated by the test surface [42]. In present study, two different types of milling machine tools viz. end mill and face mill are inspected for the presence of edge chipping and crack, respectively, using the digital holographic camera (DHC). Applicability of the camera for on-machine inspection is demonstrated by inspecting an end mill attached to a vertical milling machine.

2 Materials and methods

2.1 Wear inspection with digital holographic interferometry

Digital holography utilizes two basic principles, i.e., interference and diffraction of light for obtaining and displaying, respectively, complete information of the test object. Information of the test object is recorded optically using the principle of interference, where an object beam is superimposed with a reference beam to create an interference pattern. The resultant intensity $I(x,y)$ of this interference pattern is represented as

$$I(x,y) = \left| \psi_{\text{obj}}(x,y) + \psi_{\text{ref}}(x,y) \right|^2, \quad (1)$$

$$I(x,y) = \left| \psi_{\text{obj}}(x,y) \right|^2 + \left| \psi_{\text{ref}}(x,y) \right|^2 + \psi_{\text{obj}}^*(x,y)\psi_{\text{ref}}(x,y) + \psi_{\text{obj}}(x,y)\psi_{\text{ref}}^*(x,y). \quad (2)$$

Here, $\psi_{\text{obj}}(x,y)$ and $\psi_{\text{ref}}(x,y)$ are complex amplitude distributions of object beam scattered from the object's surface and reference beam, respectively, at any point (x,y) on the recording sensor plane. First two terms on the right-hand side in Eq. (2), i.e., $\left| \psi_{\text{obj}}(x,y) \right|^2$ and $\left| \psi_{\text{ref}}(x,y) \right|^2$ are constant terms, and $\psi_{\text{obj}}^*(x,y)$ is the complex conjugate of the object beam. The equations for object and reference beams can be represented as

$$\psi_{\text{obj}}(x,y) = \Psi_A(x,y) \exp(-j\varphi_A(x,y)), \quad (3)$$

$$\psi_{\text{ref}}(x,y) = \Psi_R(x,y) \exp(-j\varphi_R(x,y)). \quad (4)$$

Here, $\Psi_A(x,y)$ and $\varphi_A(x,y)$ are amplitude and phase distributions of object beam; $\Psi_R(x,y)$ and $\varphi_R(x,y)$ are amplitude and phase distributions of reference beam. The resultant intensity governed by Eq. (2) can be represented as

$$I(x,y) = \Psi_A^2 + \Psi_R^2 + 2\Psi_A\Psi_R \cos(\varphi_R(x,y) - \varphi_A(x,y)). \quad (5)$$

Here, first two terms on right hand side Ψ_A^2 and Ψ_R^2 are constant terms and third term represent amplitude modulation ($\Psi_A\Psi_R$) and phase modulation $\varphi_R(x,y) - \varphi_A(x,y)$ of light scattered from test object. This interference pattern is recorded using a digital sensor array such as charge-coupled device (CCD), and complementary metal oxide semiconductor (CMOS). The recorded interference pattern is known as digital hologram, which is stored in a personal computer for further numerical processing. The wavefront recorded in digital holograms, can be reconstructed numerically using different methods of wave propagation based on scalar diffraction theory, e.g., Rayleigh–Sommerfeld [43], angular spectrum [44], Fresnel diffraction [45], convolution [46] etc. In present work, Fresnel diffraction method (FDM) is used for numerical reconstruction of wavefront of test object stored in digital holograms, because FDM fulfils the Nyquist criterion [47, 48] for the given sizes of the objects (18 mm and 50 mm) and the recording distance (250 mm from recording sensor). The Fresnel diffraction equation for numerical computation of wavefront at propagation distance 'z' is represented as

$$\psi(\eta, \xi, z) = \frac{\exp(-jkz)}{j\lambda z} \exp\left(\frac{j\pi(\eta^2 + \xi^2)}{\lambda z}\right) \times \text{FT} \left[I(x,y) \exp\left(\frac{j\pi(x^2 + y^2)}{\lambda z}\right) \right]. \quad (6)$$

Here, $\psi(\eta, \xi, z)$ represents the complex amplitude distribution of wavefront of object at any point (η, ξ) on reconstruction plane, obtained by propagating the recorded field $I(x,y)$ from recording sensor plane to distance z ; k is the wave number; λ is the source wavelength; and $j = \sqrt{-1}$. In the DHI process, two digital holograms of the test object are

recorded corresponding to its two different states obtained through the process of external loading. The path length of the object beam changes due to applied external load. Complex amplitude of object wavefront is computed numerically from recorded digital hologram using Fresnel diffraction Eq. (6). Two separately computed complex amplitudes $\psi_1(x, y, z)$ and $\psi_2(x, y, z)$, corresponding to two different states of the object, are numerically subtracted to give DHI results as

$$\psi_s(x, y, z) = \psi_2(x, y, z) - \psi_1(x, y, z). \tag{7}$$

Here, $\psi_s(x, y, z)$ is the complex amplitude obtained after subtraction. The amplitude distribution is obtained by calculating the absolute (*abs*) value of $\psi_s(x, y, z)$ as

$$A_\psi = \text{abs}(\psi_s(x, y, z)). \tag{8}$$

The amplitude distribution A_ψ is useful for qualitative analysis, because any wear present on the test object may result in abrupt discontinuity in the interferometric fringes obtained after subtraction. These fringes represent change in test object’s state caused by external loading. The discontinuity in fringes also helps in visually locating the position of wear or crack on the test object. Apart from qualitative analysis, quantification of lateral dimensions and location of wear is also one of the merits of DHI. For quantitative analysis, modulo- 2π phase map is computed by numerically subtracting the arguments (*arg*) of the complex amplitudes $\psi_1(x, y, z)$ and $\psi_2(x, y, z)$ as represented in Eq. (9):

$$\Delta\phi_\psi = \arg \{ \psi_2(x, y, z) \} - \arg \{ \psi_1(x, y, z) \}, \tag{9}$$

where $\arg(X) = \tan^{-1} \{ \text{Im}(X)/\text{Re}(X) \}$; and $\Delta\phi_\psi$ is the modulo- 2π phase, which represents change in phase of object beam occurred due to applied external load. $\Delta\phi_\psi$ is also known as wrapped phase as it is limited in the interval $-\pi$ to π . This restriction results in artificial jump of phase at interval of 2π [49]. Phase unwrapping is required to remove the 2π phase ambiguity imparted by two-dimensional arctangent function used to calculate the phase from a complex valued intensity. The two-dimensional phase unwrapping algorithm used in the present work is based on Goldstein’s branch-cut method [50] to obtain continuous phase map for quantitative analysis. In this method, the algorithm identifies residues (local phase errors caused by noise) and removes them by connecting the positive and negative residues using branch-cuts. Thus, this method avoids the inconsistency during phase estimation. Three dimensional surface map can be obtained from unwrapped phase using the following equation [38]:

$$d(x, y) = \frac{\lambda}{2\pi(1 + \cos \theta)} \Delta\phi_u(x, y). \tag{10}$$

Here, $d(x, y)$ is the out-of-plane displacement caused by external load and is made explicit through unwrapped phase difference $\Delta\phi_u(x, y)$ at any point (x, y) on object’s surface; and θ is the angle between the direction of source (illumination) and direction of recording sensor (observation). Lateral dimensions of the wear are obtained by generating a 2D profile across surface map obtained using Eq. (10), at the position of wear. Number of pixels covered by the wear along the profile is multiplied by the pixel pitch at reconstruction plane. The change in pixel pitch, given by Eq. (11), during propagation of object wavefront using Fresnel diffraction method (Eq. 6), is accounted for calculation of lateral dimensions of machine tools and wear [51]:

$$\Delta_x = \frac{\lambda z}{N\Delta\xi}; \quad \Delta_y = \frac{\lambda z}{M\Delta\eta}. \tag{11}$$

Here, Δ_x and Δ_y are values of pixel pitch on image reconstruction plane corresponding to recording sensor’s pixel pitch $\Delta\xi$ and $\Delta\eta$; N and M represent number of pixels of recording sensor array along x - and y -directions, respectively; λ is the source wavelength, and z is the propagation distance.

2.2 Experimental setup

An indigenously developed portable digital holographic camera (DHC) is employed to record digital holograms of machine tools. A schematic representation of the optical arrangement of the DHC [38] is shown in Fig. 1a. The machine tools tested using DHC include square shoulder face mill and cylindrical shank solid end mill tools, as shown in Fig. 1b, c, respectively.

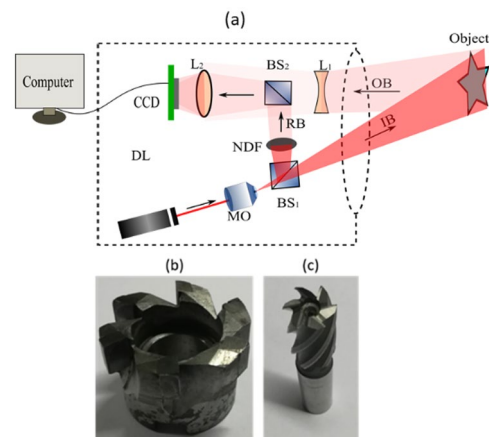


Fig. 1 a Schematic representation of the optical arrangement of digital holographic camera, where DL diode laser, MO microscope objective, BS beam splitter, OB object beam, IB illumination beam, RB reference beam, NDF neutral density filter, L1 concave lens, L2 convex lens, CCD charge-coupled device, b square shoulder face mill, and c cylindrical shank solid end mill machine tools used for inspection.

These machine tools having diameters of 18 mm (end mill tool) and 50 mm (face mill tool), are made of high-speed steel material. DHC employs an off-axis digital holographic experimental setup in which a diode laser (wavelength—660 nm, power—30 mW) is used as coherent source. A 60 \times microscope objective expands the beam from laser source. The expanded laser beam is divided into two parts by a 50:50 cube beam splitter. The transmitted beam illuminates the test object's surface and gets scattered from it to form the object beam. The reflected beam from beam splitter forms the reference beam, which is combined with the object beam by another 50:50 cube beam splitter. A neutral density filter placed in the path of reference beam controls its intensity. DHC utilizes combination of a concave lens ($f/2$) and convex lens ($f/3.2$) in the path of object beam. This lens combination serves the purpose of making the DHC compact and portable and also to record larger area at smaller object-to-sensor distances as compared to traditional digital holographic setups. The object beam and reference beam are superimposed to create an interference pattern which is recorded by a charge-coupled device (CCD) image sensor (resolution: 3376 \times 2704; pixel pitch: 3.1 $\mu\text{m} \times$ 3.1 μm). The size of the constructed DHC is 243 mm \times 103 mm \times 115 mm ($l \times b \times h$). The DHC contains all the optical and optomechanical components including laser source and CCD inside a mechanical housing.

3 Results and discussion

3.1 Wear inspection of end mill tool

The end mill tool, photograph shown in Fig. 1c, is tested for presence of wear, i.e., chipping of edges, using the DHC. Thermal load is applied using an incandescent lamp in the process of DHI. The results obtained with DHI process are shown in Fig. 2.

The amplitude distribution calculated using Eq. (8) is shown in Fig. 2a, where localized intensity variation can be observed around the damaged edges of the tool, as encircled 1 and 2 in Fig. 2a and enlarged in Fig. 2b. The unwrapped phase map shown in Fig. 2c, is obtained by applying Goldstein's unwrapping method on modulo- 2π phase calculated using Eq. (9). Wear on the edge at one of the flutes of the end mill tool, indicated by rectangle in Fig. 2c, is shown in enlarged image in Fig. 2d. Furthermore, 3D surface map of the end mill tool, depicted in Fig. 2e, is generated using Eq. (10). Parameters along x - and y -axes show the lateral dimensions of the edges and parameter along z -axis represents the displacement caused by thermal loading of the tool during DHI process. The colormap in Fig. 2e represents the variation in displacement of tool's surface due to thermal load. The size of the edge of the flute of end mill tool shown

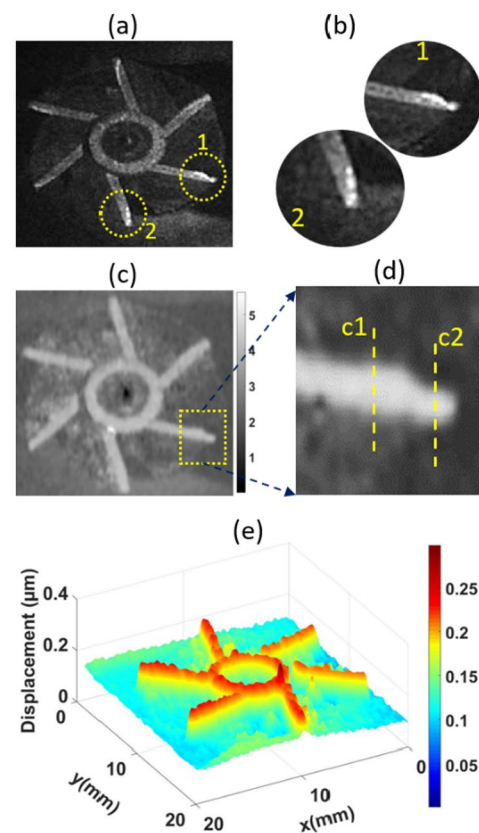


Fig. 2 DHI results of end mill tool: **a** amplitude distribution, **b** enlarged image of edges encircled 1 and 2 in **a**, **c** unwrapped phase map, **d** enlarged image of wear (chipping of edge) corresponding to the rectangle indicated in **c**, and **e** 3D surface map obtained using Eq. (10)

in Fig. 2d, is measured along dashed lines $c1$ and $c2$. 2D profiles generated along $c1$ and $c2$ are shown in Fig. 3.

The profiles are created by multiplying number of pixels N' and N'' covered by $c1$ and $c2$, respectively, with pixel pitch at reconstruction plane (Δ_x and Δ_y). Since, the pixel pitch changes with reconstruction distance in FDM according to Eq. (11), the values of pixel pitch at reconstruction plane in this experiment are 29.6 $\mu\text{m} \times$ 37 μm . The pixels are counted along y -axis as indicated by dashed lines in Fig. 2d. Therefore, widths corresponding to $c1$ and $c2$ becomes $N'\Delta_y$ and $N''\Delta_y$, respectively. The width along $c1$ is 1.45 mm and along $c2$ is 0.89 mm. Reduction in width of edge along $c2$ as compared to $c1$ is clearly noticed in Fig. 3. As per ISO standard ISO8688-2(1989) [52], the failure criteria for the end mill tool corresponds to the chipping width of 0.5 mm, which represents the critical value of wear. This means that if the change in flute's width of solid end mill is more than 0.5 mm, the tool becomes unusable. In present case, the tool wear is 1.45–0.89 mm = 0.56 mm, which is higher than critical value of wear and thus the tool can be categorised as unusable.

3.2 Crack and wear inspection in face mill tools

In another experiment, a different machine tool, i.e., a square shoulder face mill tool, photograph shown in Fig. 1b, is tested for the presence of deformity, using digital holographic camera. The results of DHI process using thermal load are shown in Fig. 4. The interferometric amplitude fringes (see in Fig. 4a) and modulo- 2π phase map (see in Fig. 4b) clearly show the flow of thermal gradient along the surface of the tool. These fringes are mostly continuous along the surface, except at the position of a crack. The discontinuity in fringes is clearly visible in modulo- 2π phase map (see in Fig. 4b) at the region of crack, as indicated by a rectangle, which is enlarged in Fig. 4c. For quantification

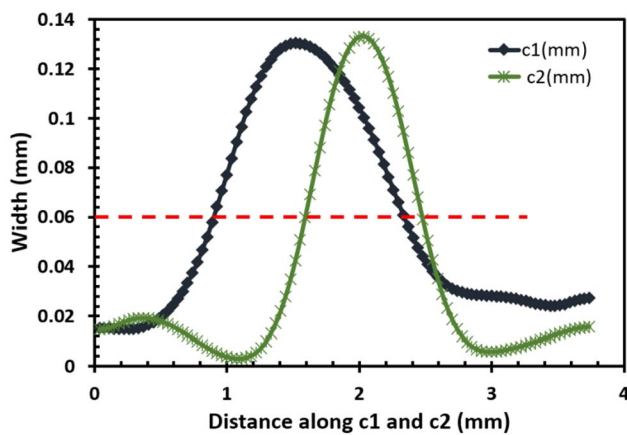
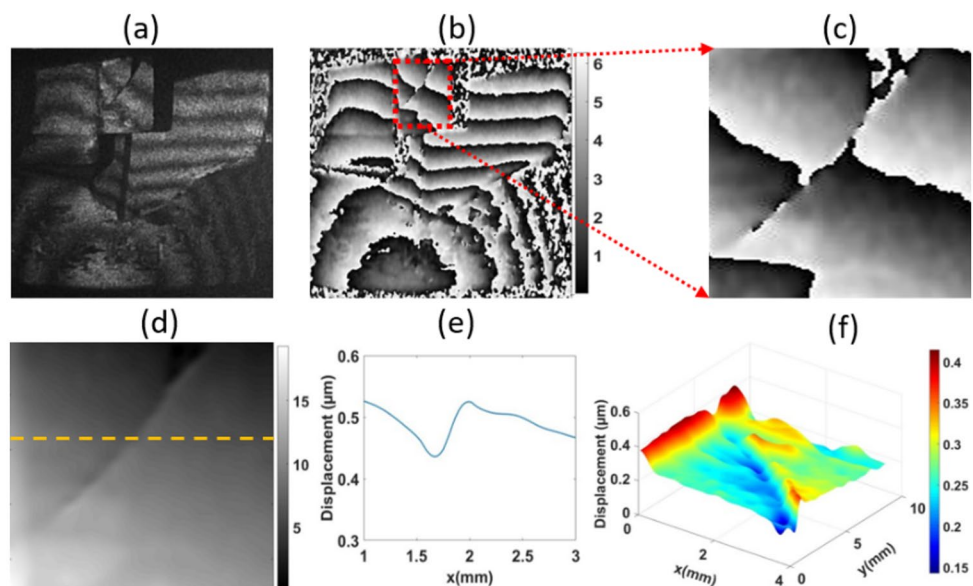


Fig. 3 2D profiles of wear occurred in the solid end mill tool, generated along dashed lines c1 and c2 indicated in Fig. 2d

Fig. 4 DHI results of square shoulder face mill tool: **a** amplitude distribution, **b** modulo- 2π phase (wrapped phase) map, **c** enlarged image of wrapped phase indicated by rectangle in **b**, **d** unwrapped phase map corresponding to **c**, **e** 2D line profile corresponding to dashed line indicated in **d**, **f** 3D surface map corresponding to **d**



of the crack, the phase map in Fig. 4c is unwrapped using Goldstein’s method. The unwrapped phase map is shown in Fig. 4d.

The lateral size of the crack is obtained from 2D line profile, shown in Fig. 4e, generated along the dashed line shown in Fig. 4d. Here also, the 2D profile is obtained by multiplying number of pixels covered by dashed line with pixel pitch at reconstruction plane (i.e., $29.7 \mu\text{m} \times 37 \mu\text{m}$). The size of the crack obtained using DHC is 0.35 mm. The crack is also measured using a standard mechanical profiler (Taylor Hobson, PGI-120) for validation. A 2D plot of the measurements obtained using mechanical profiler is shown in Fig. 5. The measured value of size of the crack using the mechanical profiler is 0.32 mm.

Thus, the measurement error in results obtained with the DHC is approximately 9% as compared to the results obtained with the mechanical profiler. The 3D surface map generated by applying Eq. (10) on the unwrapped phase map is shown in Fig. 4f. The presence of crack is analogous to the sudden change in colormap (blue colour) at the position of the crack. One of reasons for development of crack in these face mill tools is their fixed and irreplaceable cutting edges. In current industrial manufacturing machines, most of the face mill tools have replaceable inserts made of materials like carbide [53] due to their higher durability. Therefore, an indexable square shoulder face mill tool with carbide insert is also inspected for wear using the DHC, as shown in Fig. 6.

The face mill tool shown in Fig. 6a is thermally loaded by an incandescent lamp. Two digital holograms acquired using DHC at different temperatures are numerically reconstructed by FDM. Figure 6b shows the amplitude distribution obtained by numerical subtraction of absolute values of complex fields obtained from the recorded digital

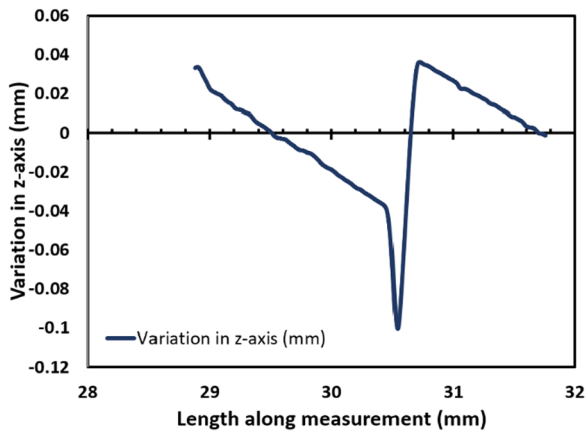


Fig. 5 2D profile along the crack region generated by standard mechanical profiler (Taylor Hobson, PGI-120)

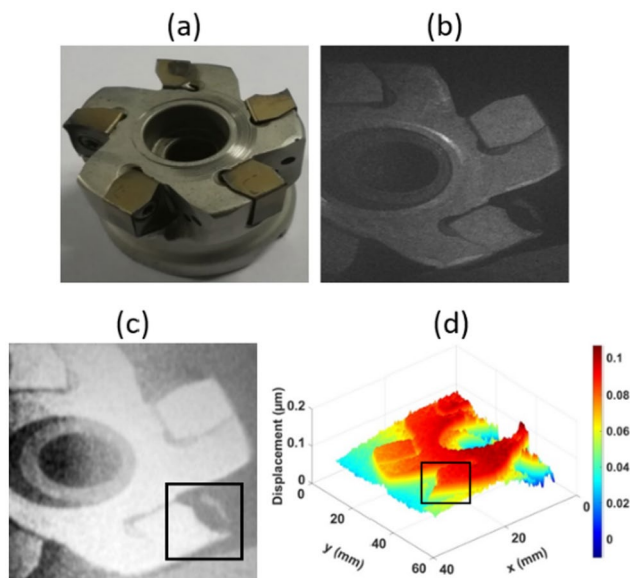


Fig. 6 **a** Photograph of indexable square shoulder face mill tool, **b** amplitude distribution, **c** unwrapped phase map, and **d** 3D surface map obtained in DHI process.

holograms. The unwrapped phase map shown in Fig. 6c is obtained by applying Goldstein's unwrapping method on modulo 2π phase distribution resulted from subtraction of the phases of the two reconstructed complex fields. From unwrapped phase map, a 3D surface map is generated using Eq. (10). The position of wear in the insert of the tool is indicated by rectangular boxes in unwrapped phase map and 3D surface map shown in Fig. 6c, d, respectively.

3.3 On-machine inspection of machine tool

In the current fast-paced industrial scenario, an important requirement for precision machining is on-machine monitoring of wear and tear in machine tools. Due to DHC's portability and capability to provide almost real time analysis, a potential application of DHC is on-machine inspection of machine tools, which is demonstrated in Fig. 7.

A solid end mill tool fixed on a vertical milling machine (HMT, FN2U) is inspected using the DHC mounted on a commercial tripod, as shown in Fig. 7a. The results of DHI are shown in Fig. 7b–e. Figure 7b, c represents amplitude distribution and unwrapped phase map of the end mill tool under test, as indicated inside rectangular box in Fig. 7a. The phase distribution of flutes numbered 1 and 2 is not uniform, as observed in Fig. 7c, and thus, their complete information cannot be obtained. This may have happened due to a small angle between the object plane and the hologram plane, due to which information of these two flutes are distributed in more than one plane. Therefore, parallelism between object and hologram planes is important for performing metrology using DHI, as it displays information of only one plane in numerical reconstruction process. The other two properly reconstructed flutes numbered 3 and 4 in Fig. 7b are used for further inspection. Figure 7d, e shows phase maps of flute numbered 4 indicated in rectangular box and its 3D displacement map, respectively. The 3D map shown in Fig. 7e also depicts shape of the flute 4 of the end mill tool. No wear in the flutes 3 and 4 are observed in DHI process.

The quality and accuracy of DHI results in on-machine inspection depends greatly on machine vibrations. Therefore, during DHI process, the machine tool under test as well as the machine itself has to be in non-operational condition. Also, steadiness of tripod and so the DHC is an important factor to be considered during the DHI process. To study the stability of the DHC during interferometric measurements, a holographic video (1.04 min duration) of the end mill tool fixed on the milling machine is recorded using the DHC in the experimental condition shown in Fig. 7a. Here, DHC was mounted on a commercial tripod. All the 1931 frames recorded in the video are extracted. Each frame represents a digital hologram. These digital holograms are utilised to perform DHI. The first frame is considered the reference frame and all other frames are compared with it. For comparison, the phase map is obtained from the complex amplitude obtained from each digital hologram after applying Fresnel diffraction method. The path length computed from the phase map of the reference frame is compared from path lengths of other 1930 frames by subtraction and unwrapping of phases. In the present case, the stability of the DHC during the measurement can be determined by variation in values of the path lengths.

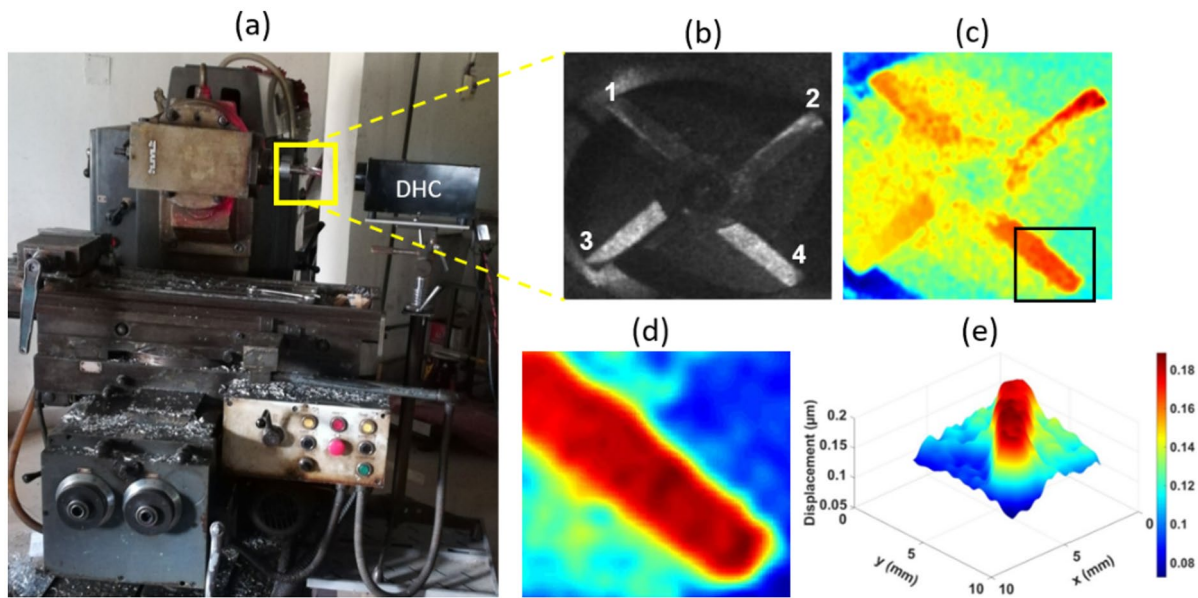


Fig. 7 **a** Photograph of on-machine inspection of end mill tool fixed on a vertical milling machine using DHC, **b** amplitude distribution of end mill tool indicated in rectangular box in **a**, **c** unwrapped phase

map of end mill tool under test, **d** phase map of one of the flutes indicated in rectangular box in **c**, **e** 3D surface map of the edge of the end mill tool shown in **d**.

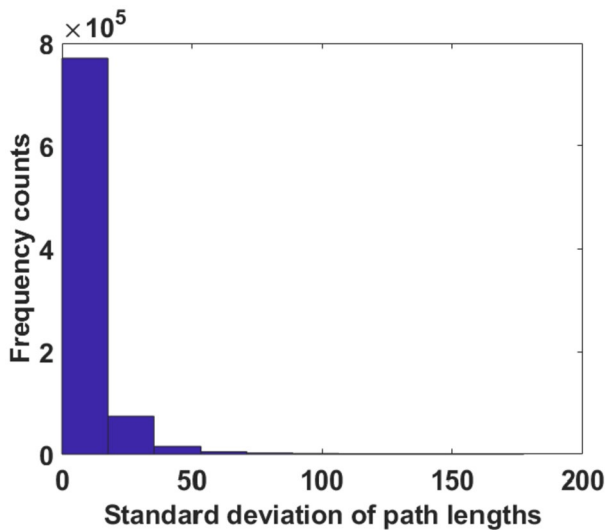


Fig. 8 Histogram of standard deviation of path length variations

Large variation in the path length over recording time would imply an unstable DHC and inaccurate measurement. Figure 8 shows a histogram of standard deviation of path length values. The variation in path values is highest in the range 0–17.7 nm and the mean is 11.86 nm, which shows very little variation in path length values. The mean value of standard deviation is obtained by calculating the mean of histogram as expressed in the following equation:

$$\text{Mean of histogram} = \frac{\text{Bin count} \times \text{Bin center}}{\text{Total number of bins}} \tag{12}$$

Here, bin represents value of path length. Thus, the stability of the DHC employed for on-machine inspection can be determined by evaluating the path lengths from the unwrapped interferometric phase obtained in the DHI process. The results obtained in this work demonstrate capability of DHI for qualitative and quantitative inspection of machine tools using the portable DHC. The 3D surface maps provide access to the lateral dimensions of the machine tool under test. Thus, apart from signifying the wear and tear in machine tools, DHC is also capable for metrology purposes due to generation of 3D surface maps in DHI process.

4 Conclusions

In summary, the presented work experimentally demonstrates a non-invasive, on-machine scheme for inspection of machine tools using optical digital holographic interferometry (DHI). An indigenously developed portable digital holographic camera was employed on the machine to record digital holograms in-situ required in the process of DHI. End mill and face mill machine tools are inspected for presence of wear and cracks. The wear and tear are analysed qualitatively as well as quantitatively using 2D profiles and 3D surface maps generated in DHI process. The measured results of the crack present in face mill machine tool are validated

by a standard mechanical profiler. Capability of the DHC to perform on-machine qualitative as well as quantitative analysis of the test object demonstrates its uniqueness in the field of non-destructive testing and metrology of machine tools. Future interests may include utilization of developed digital holographic camera for on-site inspection of different types of tools in machines like bore, grinder, drill, power saw etc.

Acknowledgements Lavlesh Pensia thanks to CSIR, New Delhi, India for financial support during the research work. Authors are thankful to Dr. Sanjeev Soni of CSIR-CSIO for technical discussion and suggestions. Authors are also thankful to Mr. Deepak Kashyap for providing experiment samples.

Author contributions Conceptualization, GD; methodology, GD; software, GD; formal analysis, GD, LP and RK; investigation, GD and LP; resources, OS; writing—original draft preparation, GD; writing—review and editing, RK; supervision, RK; project administration, RK; funding acquisition, RK. All authors have read and agreed to the published version of the manuscript.

Funding This research received no external funding.

Data availability The data related to the study reported in this manuscript are available with the corresponding author upon reasonable request.

Declarations

Conflict of interest RK, GD and OS are inventors on a patent describing method and system for recording digital holograms of larger objects in non-laboratory environment [US patent application number 16/912604; India patent application number 201911023585].

References

- A. Akcay, E. Topan, G.-J. van Houtum, *IIEE Trans.* **53**, 74 (2021)
- J.S. Chen, C.C. Ling, *Int. J. Adv. Manuf. Technol.* **11**, 198 (1996)
- T.M. El-Hossainy, *Mater. Manuf. Process.* **16**, 165 (2001)
- S. Selvakumar, V.S. Sreebalaji, K. Ravikumar, *Mater. Manuf. Process.* **36**, 792 (2021)
- X. Guo, C. Lee, *J. Manuf. Process.* **64**, 1214 (2021)
- D.A. Stephenson, J.S. Agapiou, *Metal Cutting Theory and Practice*, 3rd edn. (CRC Press, Taylor & Francis Group, Boca Raton, 2018)
- K.M. Fong, X. Wang, S. Kamaruddin, M.-Z. Ismadi, *Measurement* **169**, 108489 (2021)
- D.H. Tien, Q.T. Duc, T.N. Van, N.-T. Nguyen, T. Do Duc, T.N. Duy, *Int. J. Adv. Manuf. Technol.* **112**, 2461 (2021)
- Y. Dai, K. Zhu, *Precis. Eng.* **52**, 183 (2018)
- Y. Li, W. Mou, J. Li, C. Liu, J. Gao, *Robot. Comput. Integr. Manuf.* **68**, 102079 (2021)
- Q. Hou, J. Sun, P. Huang, *Int. J. Adv. Manuf. Technol.* **101**, 2415 (2019)
- J. Yu, X. Cheng, L. Lu, B. Wu, *Measurement* **182**, 109683 (2021)
- L. Čerče, F. Pušavec, J. Kopač, *J. Mech. Sci. Technol.* **29**, 3885 (2015)
- L. Čerče, F. Pušavec, J. Kopač, *Stroj. Vestnik/J. Mech. Eng.* **61**, 489 (2015)
- D. Du, J. Sun, S. Yang, W. Chen, *Int. J. Manuf. Res.* **13**, 168 (2018)
- A. Devillez, S. Lesko, W. Mozer, *Wear* **256**, 56 (2004)
- J.C. Liu, G.X. Xiong, *Appl. Mech. Mater.* **670–671**, 1194 (2014)
- A. Malakizadi, H. Gruber, I. Sadik, L. Nyborg, *Wear* **368–369**, 10 (2016)
- P. Zapico, D. Blanco, C. Cuervo, G. Valiño, J.C. Rico, *Proc. Manuf.* **13**, 13 (2017)
- M. Prakash, M. Kanthababu, *Mach. Sci. Technol.* **17**, 209 (2013)
- R.H.L. da Silva, M.B. da Silva, A. Hassui, *Mach. Sci. Technol.* **20**, 386 (2016)
- N. Arunkumar, A. Thanikasalam, V. Sankaranarayanan, E. Senthilkumar, *Mater. Manuf. Process.* **33**, 1751 (2018)
- U. Schnars, *J. Opt. Soc. Am. A* **11**, 2011 (1994)
- G. Dwivedi, A. Sharma, O. Singh, P.K. Baghel, R. Kumar, *Opt. Eng.* **59**, 102417 (2020)
- S. Verma, S.S. Sarma, R. Dhar, Rajkumar, *Optik (Stuttg.)* **126**, 3283 (2015)
- F. Vincitorio, L. Bahuer, M.P. Fiorucci, A.J. López, A. Ramil, *Optik (Stuttg.)* **163**, 43 (2018)
- F.M. Santoyo, G. Pedrini, S. Schedin, H.J. Tiziani, *Meas. Sci. Technol.* **10**, 1305 (1999)
- P. Xia, S. Ri, Q. Wang, H. Tsuda, *Opt. Express* **26**, 12594 (2018)
- G. Dwivedi, R. Kumar, in *Prog. Optomechanics. Springer Proc. Physics*, vol. 249, ed. by I. Bhattacharya, Y. Otani, P. Lutz, S. Cherukulappurath (Springer, Singapore, 2020), pp. 53–64.
- V. Lédl, P. Psota, F. Kaván, O. Matoušek, P. Mokrý, *Appl. Opt.* **56**, 7808 (2017)
- M.P. Georges, J.-F. Vandenrijt, C. Thizy, I. Alexeenko, G. Pedrini, B. Vollheim, I. Lopez, I. Jorge, J. Rochet, W. Osten, *Opt. Express* **22**, 25517 (2014)
- P. Tankam, P. Picart, *Opt. Lasers Eng.* **49**, 1335 (2011)
- T. Kreis, *IEEE Trans. Ind. Inform.* **12**, 240 (2016)
- K.A. Stetson, *Exp. Tech.* **40**, 483 (2016)
- D. Pantelić, S. Savić-Šević, D. Vasiljević, B. Murić, L. Blažić, M. Nikolić, B. Panić, *Mater. Manuf. Process.* **24**, 1142 (2009)
- L. Pensia, G. Dwivedi, R. Kumar, *Wood Sci. Technol.* **55**, 873 (2021)
- L. Pensia, G. Dwivedi, O. Singh, R. Kumar, *Appl. Opt.* **61**, B181 (2022)
- R. Kumar, G. Dwivedi, O. Singh, *Opt. Lasers Eng.* **137**, 106359 (2021)
- G. Dwivedi, L. Pensia, S.K. Debnath, R. Kumar, *Appl. Opt.* **60**, A120 (2021)
- J.W. Goodman, R.W. Lawrence, *Appl. Phys. Lett.* **11**, 77 (1967)
- M. Paturzo, V. Pagliarulo, V. Bianco, P. Memmolo, L. Miccio, F. Merola, P. Ferraro, *Opt. Lasers Eng.* **104**, 32 (2018)
- U. Schnars, W.P.O. Jüptner, *Meas. Sci. Technol.* **13**, R85 (2002)
- F. Shen, A. Wang, *Appl. Opt.* **45**, 1102 (2006)
- K. Matsushima, *Opt. Express* **18**, 18453 (2010)
- U. Schnars, T.M. Kreis, W.P.O. Jüptner, *Opt. Eng.* **35**, 977 (1996)
- J. Li, P. Tankam, Z. Peng, P. Picart, *Opt. Lett.* **34**, 572 (2009)
- T.C. Poon, J.P. Liu, *Introduction to Modern Digital Holography with MATLAB* (Cambridge University Press, New York, 2014)
- G. Dwivedi, S.K. Debnath, B. Das, R. Kumar, *J. Opt.* **49**, 118 (2020)
- J. Martinez-Carranza, K. Falaggis, T. Kozacki, *Appl. Opt.* **56**, 7079 (2017)
- R.M. Goldstein, H.A. Zebker, C.L. Werner, *Radio Sci.* **23**, 713 (1988)
- P. Ferraro, S. De Nicola, G. Coppola, A. Finizio, D. Alfieri, G. Pierattini, *Opt. Lett.* **29**, 854 (2004)
- ISO Stand. 8688-2 (1989).
- A. Saini, B.S. Pabla, S.S. Dhami, *Mater. Manuf. Process.* **35**, 598 (2020)

Publisher's Note Springer Nature remains neutral with regard to jurisdictional claims in published maps and institutional affiliations.